OXFORD

SOT | Society of Toxicology
www.toxsci.oxfordjournals.org

TOXICOLOGICAL SCIENCES, 159(2), 2017, 422–435

doi: 10.1093/toxsci/kfx142
Advance Access Publication Date: July 14, 2017
Research Article

Metabolism Modulation in Different Organs by Silver Nanoparticles: An NMR Metabolomics Study of a Mouse Model

Ivana Jarak,* Joana Carrola,* António S. Barros,* Ana M. Gil,* Maria de Lourdes Pereira,† Maria Luisa Corvo,‡ and Iola F. Duarte*,[1]

*Department of Chemistry; and †Department of Biology, CICECO – Aveiro Institute of Materials, University of Aveiro, 3810-193 Aveiro, Portugal; and ‡Research Institute for Medicines (iMed.ULisboa), Faculdade de Farmácia, Universidade de Lisboa, Lisboa 1649-003, Portugal

[1]To whom correspondence should be addressed at Department of Chemistry, CICECO - Aveiro Institute of Materials, Technological Laboratories, Campus de Santiago, University of Aveiro, 3810-093 Aveiro, Portugal. Fax: +351-234-401-470. E-mail: ioladuarte@ua.pt.

ABSTRACT

Although silver nanoparticles (AgNPs) are widely disseminated and show great potential in the biomedical field, there is a recognized need to better understand their action at the metabolic and functional levels. In this work, we have used NMR metabolomics, together with conventional clinical chemistry and histological examination, to characterize multi-organ and systemic metabolic responses to AgNPs intravenously administered to mice at 8 mg/kg body weight (a dose not eliciting overt toxicity). The major target organs of AgNPs accumulation, liver and spleen, showed the greatest metabolic changes, in a clear 2-stage response. In particular, the liver of dosed mice was found to switch from glycogenolysis and lipid storage, at 6 h postinjection, to glycogenesis and lipolysis, at subsequent times up to 48 h. Moreover, metabolites related to antioxidative defense, immunoregulation and detoxification seemed to play a crucial role in avoiding major hepatic damage. The spleen showed several early changes, including depletion of several amino acids, possibly reflecting impairment of hemoglobin recycling, while only a few differences remained at 48 h postinjection. In the heart, the metabolic shift towards TCA cycle intensification and increased ATP production possibly reflected a beneficial adaptation to the presence of AgNPs. On the other hand, the TCA cycle appeared to be down regulated in the lungs of injected mice, which showed signs of inflammation. The kidneys showed the mildest metabolic response to AgNPs. Overall, this study has shown that NMR metabolomics is a powerful tool to monitor *in vivo* metabolic responses to nanoparticles, revealing unforeseen effects.

Key words: silver nanoparticles (AgNPs); NMR metabolomics; BALB/c mice; *in vivo*; metabolism; nanotoxicity.

Silver nanoparticles (AgNPs) are one of the classes of nanomaterials with largest production and commercialization (Tran *et al.*, 2013). Due to their well-documented antimicrobial properties, AgNPs are currently incorporated into numerous consumer goods, including textiles, cosmetics and food packaging materials, as well as in medical products, such as wound dressings, implants and catheters (Ge *et al.*, 2014). Moreover, new therapeutic applications are increasingly being explored based on other interesting biological properties of AgNPs, such as antiviral or anticancer activities (Wei *et al.*, 2015). One of the advantageous features of AgNPs is their ability to gradually release silver ions, in a controlled and tunable manner, enabling long-term biological activity. Also, upon surface functionalization, AgNPs can be designed to target specific cells or intracellular components, functioning as a reservoir of silver ions or other bioactive species that can be selectively delivered. Thus, the potential of AgNPs in the biomedical field is immense. On the other hand, there is a recognized need to better define the potential adverse effects of AgNPs to human health, and to understand their mechanisms of action in eukaryotic cells and higher

organisms. Numerous toxicity studies have been published over the last years, using either *in vitro* cellular models or *in vivo* animal assays (Dubey *et al.*, 2015; Kim and Ryu, 2013). The studies in rodents like mice and rats have been particularly useful to address the *in vivo* fate of AgNPs and their accumulation in different organs (eg, Dziendzikowska *et al.*, 2012; Xue *et al.*, 2012). Some of these studies have also revealed toxic effects for AgNPs, based mainly on serum biochemical parameters and histopathological examination of main organs (eg, De Jong *et al.*, 2013; Recordati *et al.*, 2016), or on genotoxicity assessments (Li *et al.*, 2014b). However, the organism's response to subtoxic doses of AgNPs at the metabolic and functional levels is still largely unknown.

Assessing the metabolic profiles of tissues and/or biofluids from animal models exposed to nanoparticles (NPs), through NMR or MS-based metabolomics, is increasingly proving its value for revealing unforeseen biological effects and helping to understand the pathophysiological perturbations induced by NPs (Duarte, 2011; Lv *et al.*, 2015). In the case of AgNPs, *in vivo* metabolomic studies have focused on the environmental impact of these particles, using a terrestrial invertebrate earthworm (Li *et al.*, 2015a) and a freshwater invertebrate (Li *et al.*, 2015b) as model organisms. However, to our knowledge, the application of metabolomics to mammalian models with a view to assess putative effects of AgNPs on human health, has been confined to one study of rat urine (Hadrup *et al.*, 2012).

In this work, we employ NMR metabolomics, together with conventional clinical chemistry and histological examination, to characterize the compositional changes of different organs (liver, spleen, kidney, heart, and lung) and blood serum of mice exposed to AgNPs. The main goal is to achieve an integrated view of local and systemic metabolic adaptations to the presence of AgNPs and of their putative relation to common toxicity readouts. Ultra-purified, 30 nm spherical AgNPs coated with polyethyleneglycol (PEG) were used. PEG, which is approved for human use in pharmaceutical products, is known to improve NP colloidal stability (Luo *et al.*, 2005) and to prevent protein adsorption, thereby promoting extended circulation in the body (Xu *et al.*, 2007). The PEG-coated AgNPs were administered through intravenous (i.v.) injection, which is the most relevant route to simulate a medical-related exposure to humans. Moreover, even if exposure occurs via nasal, oral, or dermal routes, AgNPs may enter the bloodstream and reach different organs (Davenport *et al.*, 2015; Hadrup and Lam, 2014; Korani *et al.*, 2011), hence the added importance of the intravenous route in regard to the safety of consumer and topical biomedical products. Three time points following injection (6, 24, and 48 h) were assessed, seeking to capture early effects of AgNPs exposure. As previous studies have shown that AgNPs i.v. injected into mice quickly disappear from the blood (within <1 h) and distribute into body organs (Chen *et al.*, 2016; Xue *et al.*, 2012), and based also on the premise that sub-toxic doses may affect the metabolism at early response stages, as demonstrated *in vitro* (Carrola et al., 2016a), we expect that this period provides an adequate time window for our study. NMR spectroscopy was the analytical platform elected for this assessment as it enables the direct analysis of intact tissues in a rapid, nondestructive way, providing qualitative and quantitative information on a wide range of metabolites involved in central metabolism.

MATERIALS AND METHODS

Silver nanoparticles. Sterile, ultra-purified and endotoxin-free AgNPs (Biopure AgNPs 1.0 mg/ml) with a core diameter of 30 nm and a methoxy(polyethylene glycol)-thiol coating (m-PEG-SH 5 kDa) were purchased from Nanocomposix Europe (Prague, Czech Republic). The specifications of the manufacturer (size, morphology and hydrodynamic diameter) were verified according to the procedures reported in our preceding work (Carrola *et al.*, 2016a). Moreover, the particle size distribution in saline was assessed by dynamic light scattering (DLS).

Animal handling and sample collection. Male BALB/c mice (24–28 g) were provided by the Instituto Gulbenkian de Ciência (Oeiras, Portugal), and kept in a well-ventilated room with regulated temperature (21°C ± 2°C), humidity (55% ± 10%) and 12-h light/12-h dark cycle. Animals were fed with standard laboratory food and acidified water *ad libitum*. All animal experiments were carried out in the authorized Animal Facilities of the Faculty of Pharmacy at the University of Lisbon, with permission of the local animal ethical committee, and in accordance with the Declaration of Helsinki, the EEC Directive (2010/63/UE) and Portuguese law (DL 113/2013, Despacho no. 2880/2015), and all related legislations for the humane care of animals in research.

For a preliminary biodistribution study, 4 mice were i.v. injected in the tail vein with 0.2 ml of AgNPs in NaCl (0.154 M), at 8 mg/kg of body weight (bw), while 2 control mice were injected with 0.2 ml of NaCl (0.154 M), 1 h prior to sample collection. The dose of AgNPs was selected based on the concentration of the stock solution available (1 mg/ml) and the maximum acceptable i.v. injection volume. The animals were anesthetized and blood was collected by puncture from the orbital cavity. Then, mice were sacrificed by cervical dislocation and the organs of interest (liver, spleen, kidney, heart, muscle, and lungs) were harvested, rinsed with cold KCl (0.154 M), dried for excess of fluid and weighted. Concentration of silver in organs and blood was determined by ICP-OES after acid digestion (approximately 50 mg/μl of tissue/blood boiled at 180 °C in 100 μl perchloric acid for 2 h). For the toxicological study, 26 mice were randomly assigned to 4 groups. The control group ($n = 9$) was administered in the tail vein with 0.2 ml of NaCl (0.154 M), 48 h prior to sample collection. The remaining animals were administered in the tail vein with 0.2 ml of AgNPs (8 mg/kg bw) in NaCl (0.154 M), and assigned to 3 experimental groups differing in exposure time: 6 h ($n = 7$), 24 h ($n = 5$), and 48 h ($n = 5$). At each postinjection time, animals were weighted, anesthetized and blood was collected by puncture from the orbital cavity. Following sacrifice (performed as described earlier), the organs were collected, rinsed with cold KCl (0.154 M), dried for excess of fluid and weighted. Collected tissues were immediately frozen in liquid nitrogen and stored at −80°C until High Resolution Magic Angle Spinning (HRMAS) NMR analysis, or in a 10% (v/v) neutral buffered formalin solution for histological studies. Due to the limited blood volume retrievable from each mouse, blood samples for hematology and clinical biochemistry were taken from only 2 dosed mice of each experimental group (and from 4 controls), while the blood of remaining animals was processed to obtain the serum for subsequent ^{1}H NMR analysis.

Histopathology. Tissue fragments of control and dosed animals were dehydrated in graded ethanol series, embedded in paraffin wax, and sectioned (4–5 μm thick) using a Leitz microtome model 1512 (Leica Biosystems, Wetzlar, Germany). Sections were double stained with hematoxylin and eosin (HE) for light microscopy. Observations and micrographs were conducted on a digital camera (Olympus Camedia C-5060) coupled to a microscope (Olympus BX41, Tokyo, Japan).

Hematology and serum biochemistry. Hematologic analysis was carried out on an ADVIA 120 Hematology System (Siemens, Erlangen, Germany). Serum biochemical parameters were determined using an ADVIA Chemistry Systems (Bayer HealthCare, New York, USA) analyser following the protocols defined in appropriate kits. Due to the small number of samples available for this analysis, the results were expressed as the lowest and highest value range and compared with the reference values reported for mice (Martins *et al.*, 2014).

Sample preparation for NMR. At the time of analysis, the frozen tissues were washed with a few drops of D_2O saline (0.9%) to remove excess blood, and about 40 mg of thawed cold tissue were packed into 50 μl HRMAS rotors, containing 10 μl of D_2O saline with 0.25% 3-(trimethylsilyl)propionate sodium salt (TSP)-d_4 to provide a signal for lock (D_2O) and for shimming (TSP). Serum samples were thawed and homogenized using a vortex mixer. Then, 400 μl of saline solution (NaCl 0.9% in 10% D_2O) was added to 200 μl of serum. After centrifugation (8000 rpm, 5 min, room temperature), 550 μl of each sample were transferred to 5 mm NMR tubes.

NMR spectroscopy. All NMR spectra were acquired on a Bruker Avance DRX-500 spectrometer operating at 500.13 MHz for ^1H observation, and using a 4mm HRMAS probe for tissue analysis and a 5 mm TXI probe for serum analysis. Tissue HRMAS NMR spectra were recorded at 277 K with a spinning rate of 4 kHz. To attenuate broad signals of macromolecules and improve the detection of small metabolites, the T_2-edited Carr-Purcell-Meiboom-Gill spin-echo pulse sequence with water presaturation ('cpmgpr1d' in Bruker library) was employed, using a total spin echo time of 64 ms ($n = 80$, $\tau = 400$ μs). Typically, 256 transients were acquired with 32 k points, spectral width of 13 ppm, relaxation delay of 4 s, and acquisition time of 2.5 s. Spectra were processed with a line broadening of 0.3 Hz and zero-filling factor of 2, manually phased and baseline corrected. Chemical shifts were referenced internally to the alanine signal at δ 1.48 ppm. For blood sera, 3 1D spectra were acquired: (1) standard 1D ^1H spectrum with water suppression ("noesypr1d") with 128 transients and mixing time of 0.1 s; (2) T_2-edited spectrum ("cpmgpr1d") with 256 transients and total spin echo of 64 ms ($n = 80$, $\tau = 400$ μs); (3) diffusion-edited spectrum ('ledbpgp2s1dpr') with 128 transients, 100 ms diffusion delay, and 0.1 s pulse-field gradient. Serum spectra were acquired at 300 K, with 32 k points, spectral width of 20 ppm, 4 s relaxation delay, and acquisition time of 1.6 s. Spectral processing comprised exponential multiplication with a line broadening of 0.3 Hz (standard 1D and T_2-edited) or 0.5 Hz (diffusion-edited), zero-filling to 64 k, manual phasing and baseline correction. Chemical shifts were referenced internally to the α-glucose signal at δ 5.23 ppm. Additionally, 2D homonuclear (TOCSY, *J*-resolved) and heteronuclear (HSQC) spectra were recorded for selected samples to help spectral assignment. The main acquisition and processing parameters for these experiments are summarized in Supplementary Table 1. Spectral assignments were based on matching the recorded 1D and 2D NMR spectra to reference data available in the Bruker Biorefcode database and other public databases such as HMDB (Wishart *et al.*, 2007), and further supported by statistical total correlation spectroscopy (Cloarec *et al.*, 2005).

Multivariate analysis and spectral integration. Spectra were aligned using recursive segment-wise peak alignment (Veselkov *et al.*, 2009) to minimize chemical shift variations, normalized by probabilistic quotient normalization (PQN) (Dieterle *et al.*, 2006) to account for dilution-independent effects on spectral area and scaled to unit variance. Data matrices were built in Amix-viewer (version 3.9.14, BrukerBiospin, Rheinstetten) using all intensity values in the δ 0.6–8.9 ppm region (excluding the suppressed water signal) and multivariate analysis (MVA) was performed in SIMCA-P11.5 (Umetrics, Umea, Sweden). Principal component analysis (PCA) was used to identify trends, clusters and outliers, followed by partial least square discriminant analysis (PLS-DA) to assess class discrimination. A 7-fold internal cross-validation was applied to assess the explained variance (R^2) and predictive power (Q^2) of PLS-DA models. The corresponding loadings were obtained by multiplying the loading weight (w) by the standard deviation of each variable, and were color-coded according to variable importance to the projection (VIP).

To assess the magnitude of metabolite variations, selected spectral peaks were integrated in Amix-viewer, and normalized by the quotient computed from PQN. For each metabolite, the magnitude of variation in AgNPs-exposed samples relatively to controls was assessed by calculating the effect size (ES), adjusted for small sample numbers, and respective standard error, according to the equations provided in the literature (Berben *et al.*, 2012). The metabolic changes with absolute ES > 0.5 (and with standard error $<$ ES) were represented in a heatmap plot colored as a of % variation with respect to controls, using the R-statistical software. Additionally, the difference between the means of the 2 groups (control and dosed) was assessed using the 2-sample *t* test (results reported at a confidence level of 95%).

RESULTS

Physicochemical Characterization of AgNPs

As shown by transmission electron microscopy (Supplementary Figure 1a), AgNPs were approximately spherical in shape and had a metallic core diameter of 26.8 ± 5.3 nm. The hydrodynamic diameter (D_h) measured by DLS was 62.1 ± 0.5 nm, with a polydispersity index (PdI) below 0.2, thus indicating reasonable monodispersion. A zeta potential of −12.1 ± 0.5 mV was found, the slightly negative surface charge contributing for colloidal stability, together with steric interactions between the polymer molecules in the coating. When dispersed in saline (the carrier solution used for injection), AgNPs kept their D_h at approximately the same value (60.1 ± 4.6 nm), although with slightly higher PdI (0.25–0.32) (Supplementary Figure 1b). This is consistent with the high colloidal stability of these NPs, provided by steric repulsions of PEG coated surfaces, as we have previously reported in cell culture medium (Carrola *et al.*, 2016b).

Preliminary Biodistribution Study

The results of silver quantification in mice blood and tissues at 1 h postinjection showed that AgNPs were circulating in the bloodstream and had been readily taken up by the different tissues (Supplementary Figure 2). The organs showing higher accumulation of silver were the liver, spleen and kidneys, followed by the heart and lungs. Based on these results, these organs (together with blood serum) were collected for NMR analysis in the subsequent toxicological study at 6, 24, and 48 h postinjection.

Animal Observation and Effect on Body and Organ Weights

A survival rate of 100% was observed in this study. No differences on general pattern behavior or bw were noted in AgNPs-dosed mice during the whole experimental period. Relative

Table 1. Relative Organ Weights, Hematological, and Serum Biochemical Parameters for Control and Dosed Mice (6, 24, and 48 h Postinjection)

Relative Organ Weight[a] (g/100 g bw)		Control (n = 9)	Dosed 6 h (n = 7)	Dosed 24 h (n = 5)	Dosed 48 h (n = 5)
Liver		5.36 ± 0.16	5.60 ± 0.57	5.69 ± 0.40*	6.05 ± 0.30*
Spleen		0.34 ± 0.04	0.37 ± 0.04	0.39 ± 0.03	0.44 ± 0.03
Kidney		1.49 ± 0.19	1.64 ± 0.04*	1.66 ± 0.07*	1.60 ± 0.04*
Heart		0.52 ± 0.03	0.51 ± 0.02	0.51 ± 0.03	0.45 ± 0.02
Lung		n.a.	n.a.	n.a.	n.a.
Hematological Parameters	**Reference[b]**	**Control (n = 4)**	**Dosed 6 h (n = 2)**	**Dosed 24 h (n = 2)**	**Dosed 48 h (n = 2)**
Red blood cells ($\times 10^6$/mm^3)	8.98–10.66	10.53–10.16	9.99, 10.16	9.95, 10.68	10.16, 10.66
Hematocrit (%)	45.8–54.8	51.2–54.3	49.8, 52.5	50, 53.9	50.8, 51.7
Mean corpuscular volume (μm^3)	45.8–54.8	50.4–51.5	49.7, 50.0	50.3, 50.5	47.7, 49.4
Mean corpuscular Hemoglobin (pg)	13.8–15.0	15.5–16.1	15.5, 16.1	14.4, 15.8	15.5, 15.8
Leucocyte formula inversion	No	No	Yes	Yes	Yes/No
Serum biochemical parameters	**Reference[b]**	**Control (n = 4)**	**Dosed 6 h (n = 2)**	**Dosed 24 h (n = 2)**	**Dosed 48 h (n = 2)**
Creatinine (mg/dl)	0.2–0.8	0.11–0.21	0.10	0.18	0.14, 0.20
Bilirubin (mg/dl)	n.a.	0.04–0.19	0.15, 0.23	0.13, 0.16	0.08, 0.10
Glucose (mg/dl)	75–140	62–152	91, 111	64, 104	110, 143
Triglycerides (mg/dl)	26–175	140–232	87, 96	100, 119	149, 153
Total cholesterol (mg/dl)	40–200	95–112	102, 107	115, 132	108, 109
HDL cholesterol (mg/dl)	>40	43.7–64.2	50.7, 66.7	70.8, 75.1	59.2, 63.4
AST (U/l)	64.0–112	110–207	152, 180	133, 172	110, 142
ALT (U/l)	31–62	31–54	31, 38	45, 52	36, 40
ALP (U/l)	36–196	37.5–49.1	46.7, 64.7	42.6, 54.7	20.7, 36.7
GGT (U/l)	0–5	1–4	2, 3	2, 4	1, 2
LDH (U/l)	n.a.	640–3665	2472, 3773	2577, 2856	2901, 2920

AST, aspartate aminotransferase, ALT, alanine aminotransferase, ALP, alkaline phosphatase, GGT, γ-glutamyl transferase, LDH, lactate dehydrogenase; n.a. not available.

[a]Relative organ weights expressed as mean ± 1.96 × SE (95% CI).

[b]Reference values for mice.

*Statistically significant differences in relation to control animals (*F*-test) are indicated for the significance level of 0.05.

organ weights are presented in Table 1. When compared with controls, relative liver weights of dosed mice were found to be significantly increased at 24 and 48 h postinjection. Relative kidney weights increased as early as 6 h postinjection and remained elevated at later time points. NP exposure did not affect the relative weights of spleen and heart, while lung weights were not determined because it was not possible to collect intact lungs for all animals.

Histopathological Analysis of Tissues

Macroscopic observations at necropsy suggested apparently normal regular anatomic structures in all organs of control and AgNPs-dosed mice. However, histological observations (Figure 1) denoted some alterations in the organs of dosed mice, with exception of heart tissue, which displayed apparently normal features. The hepatic tissue of dosed mice showed degenerative lesions, namely cytoplasmic vacuolation of hepatocytes, which were particularly expressive at 24 h postinjection. Splenic sections of the same animals revealed a disorganized pattern of pulps (vacuolation and cell depletion within the red pulp), at both 24 and 48 h periods, these alterations being more prominent at 48 h. On the other hand, renal sections showed no microscopic changes at 24 h, while at 48 h, degenerative changes within the glomerulus were noted in dosed mice. In addition, the lumen of most tubules were closed by sloughing of epithelial cells. The histology findings of lungs revealed hemorrhage, thickening of the alveolar wall, and alveolar cavities filled with both erythrocytes and inflammatory cells, at 24 and 48 h postinjection.

Hematology and Serum Biochemistry

The hematological and serum biochemical parameters obtained for control and dosed mice are shown in Table 1. Comparison to reference values available for mice and to experimental control animals was performed to reveal variation trends upon AgNPs exposure. Red blood cell and coagulation parameters of dosed mice fell within normal values, whereas some changes were apparent in the count of white blood cells, namely a decrease in lymphocytes and an increase in neutrophils (leucocyte formula inversion), compared with control animals. In regard to biochemical parameters, serum enzymes, creatinine, bilirubin, and glucose did not show relevant differences, while triglycerides and high-density lipoprotein (HDL) cholesterol showed, respectively, decreasing and increasing trends in dosed animals compared with controls (especially at 24 h). Still, the final values remained within reference intervals.

Alterations in the Metabolome of Animal Tissues

Figure 2 shows typical ^{1}H NMR spectra (δ 4.9–0.5 ppm subregion) of the different tissues analyzed. The complete spectral assignment of all tissue profiles is presented in Supplementary Table 2. In total, near 60 compounds were identified, including several amino acids and derivatives, organic acids, choline compounds, nitrogenous bases, and nucleosides/nucleotides. Lipid signals arising mainly from fatty acyl chains and the glycerol backbone in triglycerides were also clearly detected in some tissues (especially in liver and, to a lesser extent, in kidney and lung). The liver profile was further characterized by prominent glucose signals and the presence of glycogen, uridine diphosphate (UDP)-glucose and adenine, not detected in the other organs. Kidney and lung were especially rich in glycine, choline-containing compounds and taurine, the latter also being

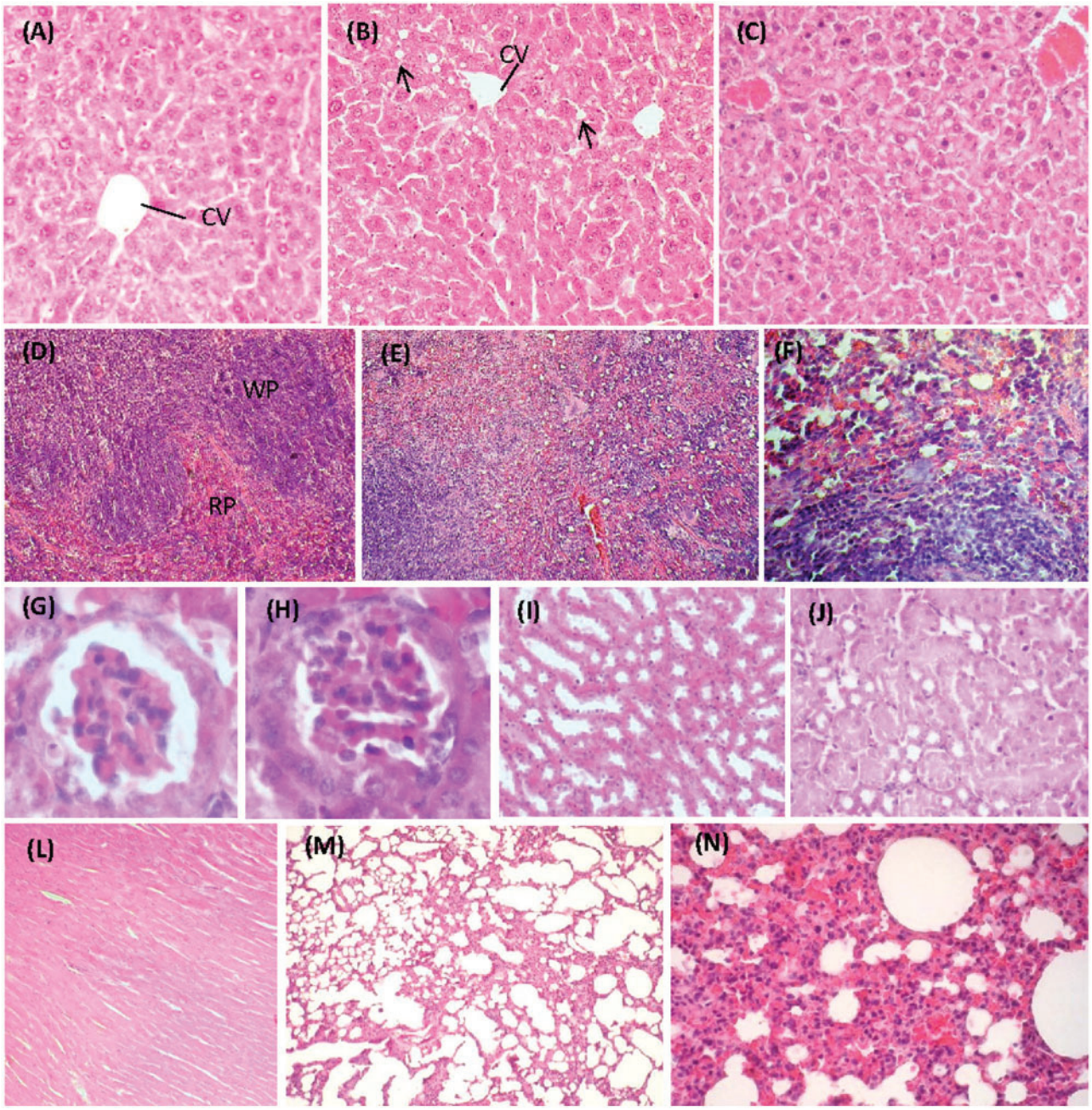

Figure 1. Histopathological changes in mice organs upon exposure to AgNPs. Representative light microphotographs of HE staining of liver, spleen, kidney, heart, and lung tissues: (A) control liver; (B) liver at 24 h postinjection, showing cytoplasmic vacuolation (arrows). CV, centrolobular vein; (C) liver at 48 h postinjection; (D) control spleen showing an organized pattern of both white (WP) and red pulp (RP); (E,F) splenic sections at 48 h postinjection, showing vacuolation and cell depletion within RP; (G) kidney glomerulus from a control mouse; (H) kidney glomerulus at 48 h postinjection, showing dilatation of Bowman's capsule, although the capillary network displays regular features; (I) control renal medullar features; (J) obstruction of lumen within renal tubules; (L) heart at 48 h postinjection, displaying normal features; (M) control lung parenchyma; (N) lung at 48 h postinjection, displaying a congested parenchyma. Original magnifications A–C,F–H: ×400; D,E,I–L,N: ×200; M: ×100.

abundantly present in heart. The spectra of heart further showed intense signals of creatine and lactate. The spleen profile was characterized by dominant signals of choline, glycerophosphocholine, betaine and *myo*-inositol, showing a unique contribution of hypoxanthine in the low field region.

In order to assess the effects of AgNPs on the metabolome of the different tissues, MVA was applied to their ^{1}H NMR profiles. The PCA scores scatter plots obtained (Supplementary Figure 3, left) revealed some grouping trends, especially for liver, heart, and lung, where one of the dosed groups (24 h for lung and 48 h for liver and heart) separated from controls. Then, at a first stage, PLS-DA was applied to discriminate between control and dosed samples (considering all exposure times together). In the resulting scores plots (Supplementary Figure 3, right), the 2 groups were reasonably separated, resulting in models with good predictive power for liver and kidney (Q^2 0.61 and 0.47, respectively), while for spleen, heart and lung, sample discrimination was less robust (Q^2 0.2–0.4), as summarized in Table 2. As suggested in some PCA and PLS-DA scores plots, exposure time could have a strong influence on the metabolic profiles, thus,

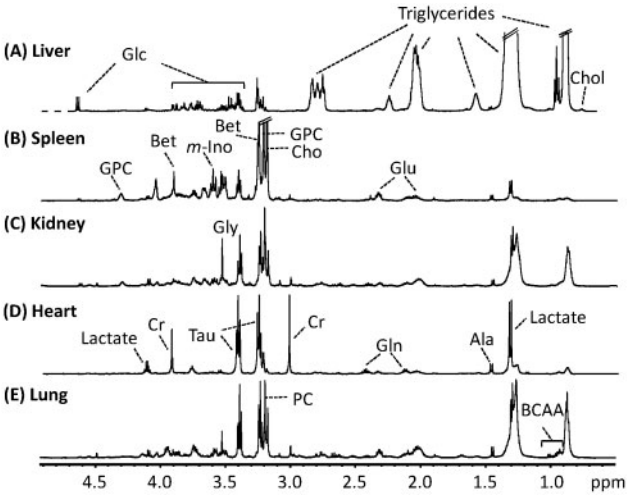

Figure 2. Typical ^{1}H T_2-edited HRMAS NMR spectra of control tissues (δ 0.5–4.9 ppm): (A) liver; (B) spleen; (C) kidney; (D) heart; (E) lung. Some assignments are indicated (complete list in Supplementary Table 2). Abbreviations: BCAA branched chain amino acids, Bet betaine, Cho choline, Chol cholesterol, Cr creatine, Glc glucose, GPC glycerophosphocholine, *m*-Ino *myo*-inositol, PC phosphocholine; 3 letter codes used for amino acids.

the next stage consisted of building PLS-DA models (control vs dosed) for each time point. Figure 3 shows the results obtained for liver, namely the scores plots and loadings, at each time point. Equivalent results for the other organs are shown in Supplementary Figures 4–7. Within each tissue type, the varying Q^2 values for the different models corroborate the importance of exposure time, with lower Q^2 values generally being obtained for the 6 h models (Table 2). The thorough analysis of loadings profiles, to highlight the main metabolites contributing for sample discrimination, was then complemented with the quantitative assessment of variations through spectral integration. The results were summarized in the form of heatmaps, color-coded as a function of % variation, where only the metabolites with absolute ES > 0.5, accepted as representative of a medium-large effect (Berben *et al.*, 2012), were included (Figure 4).

When compared with controls, dosed animals showed several alterations in the metabolic profile of liver, readily highlighted in the PLS-DA loadings (Figure 3) and confirmed through univariate analysis of signal integrals. At 6 h postinjection, glucose, glycogen, hypotaurine, and betaine were decreased (blue patches in the heatmap of Figure 4A), whereas lipids, cholesterol, choline compounds, and ascorbate were increased (yellow/orange patches in Figure 4A). Interestingly, some of these variations were reversed for longer exposures, namely the changes in glycogen and glucose (increased in 24- and 48 h-exposed mice) and in lipids (decreased in 24- and 48 h-exposed animals). Moreover, a number of changes not detected at 6 h were additionally seen at 24/48 h, namely the increases in uridine di/triphosphate (UDP/UTP), glutamine, reduced glutathione (GSH) and taurine.

The spleen metabolic composition also showed marked alterations upon AgNPs exposure (Supplementary Figs. 4 and 4B). Early effects seen at 6 h postinjection were mainly reflected on the levels of several amino acids (glycine, alanine, lysine, branched chain, and aromatic amino acids), GSH, ascorbate, acetate and malonate, all decreased compared with controls. At 24 h postinjection, additional significant decreases were seen for glutamine and myo-inositol, while trimethylamine strongly increased. A trend for increased oxidized glutathione (GSSG) was also suggested in the PLS-DA loadings (Supplementary Figure 4, middle plot), although this could not be quantified due to severe overlap. Notably, several of these changes were attenuated or disappeared at 48 h postinjection, while others remained. Additionally, a significant increase in splenic glucose was seen at this later time point.

Table 2. Summary of PLS-DA Parameters (R^2X and R^2Y Expressing Explained Variance and Q^2 Expressing Predictive Power) of Models Built for Discriminating Samples From Control and Dosed Mice, Considering: (1) All Postinjection Periods in the Dosed Class, (2) Each Period at a Time

	(1)				(2)		
Tissue	R^2X	R^2Y	Q^2		R^2X	R^2Y	Q^2
Liver	0.41	0.81	0.61	6 h	0.40	0.91	0.53
				24 h	0.43	0.90	0.53
				48 h	0.52	0.95	0.77
Spleen	0.22	0.93	0.34	6 h	0.25	0.97	0.22
				24 h	0.33	0.97	0.65
				48 h	0.26	0.97	0.41
Kidney	0.23	0.92	0.47	6 h	0.31	0.95	0.49
				24 h	0.29	0.97	0.60
				48 h	0.33	0.97	0.58
Heart	0.24	0.86	0.21	6 h	0.28	0.98	0.41
				24 h	0.28	0.97	0.43
				48 h	0.36	0.96	0.57
Lung	0.24	0.93	0.39	6 h	0.26	0.98	−0.11
				24 h	0.35	0.98	0.64
				48 h	0.35	0.98	0.58
Serum[a]	0.24/0.26	0.98/0.97	0.72/0.64	6 h	0.35/0.35	0.99/0.99	0.71/0.71
				24 h	0.44/0.48	0.99/0.99	0.86/0.85
				48 h	0.46/0.38	0.99/0.99	0.82/0.79

[a]Values for models built with T_2-edited/diffusion-edited spectra.

Within the organs assessed, the kidney was the least affected by AgNPs exposure. Indeed, within the metabolites suggested to be altered through PLS-DA loadings inspection (Supplementary Figure 5), only 4 showed statistically significant differences between control and dosed animals (Figure 4C). Hypotaurine, acetate and trimethylamine were decreased at 6 h postinjection, while an additional decrease in phosphocholine was seen at 48 h. The 24 h kidney profile of dosed animals was very similar to controls.

The impact of AgNPs on mice heart was mainly seen at 48 h postinjection, while only a few shorter-term effects were detected (Supplementary Figs. 6 and 4D). When compared with the control profile, 48 h-exposed heart showed: decreased levels of polyunsaturated fatty acids, lactate, succinate and malonate and increased levels of fumarate and ATP.

Finally, the metabolic profile of lung tissue was hardly changed at 6 h postinjection, in accordance with the negative Q^2 value of the corresponding PLS-DA model, and showed the strongest shift in relation to control animals at 48 h postinjection (Supplementary Figs. 7 and 4E). The main variations were decreases in lactate and succinate, together with increases in alanine, glutamate, and creatine.

Alterations in the Metabolome of Blood Serum

Given the high degree of spectral overlap between serum macromolecular components (eg, lipoproteins, glycoproteins) and small metabolites, the analysis of the serum metabolome has been conducted using T_2-edited spectra to assess the variations in small metabolites and diffusion-edited spectra to

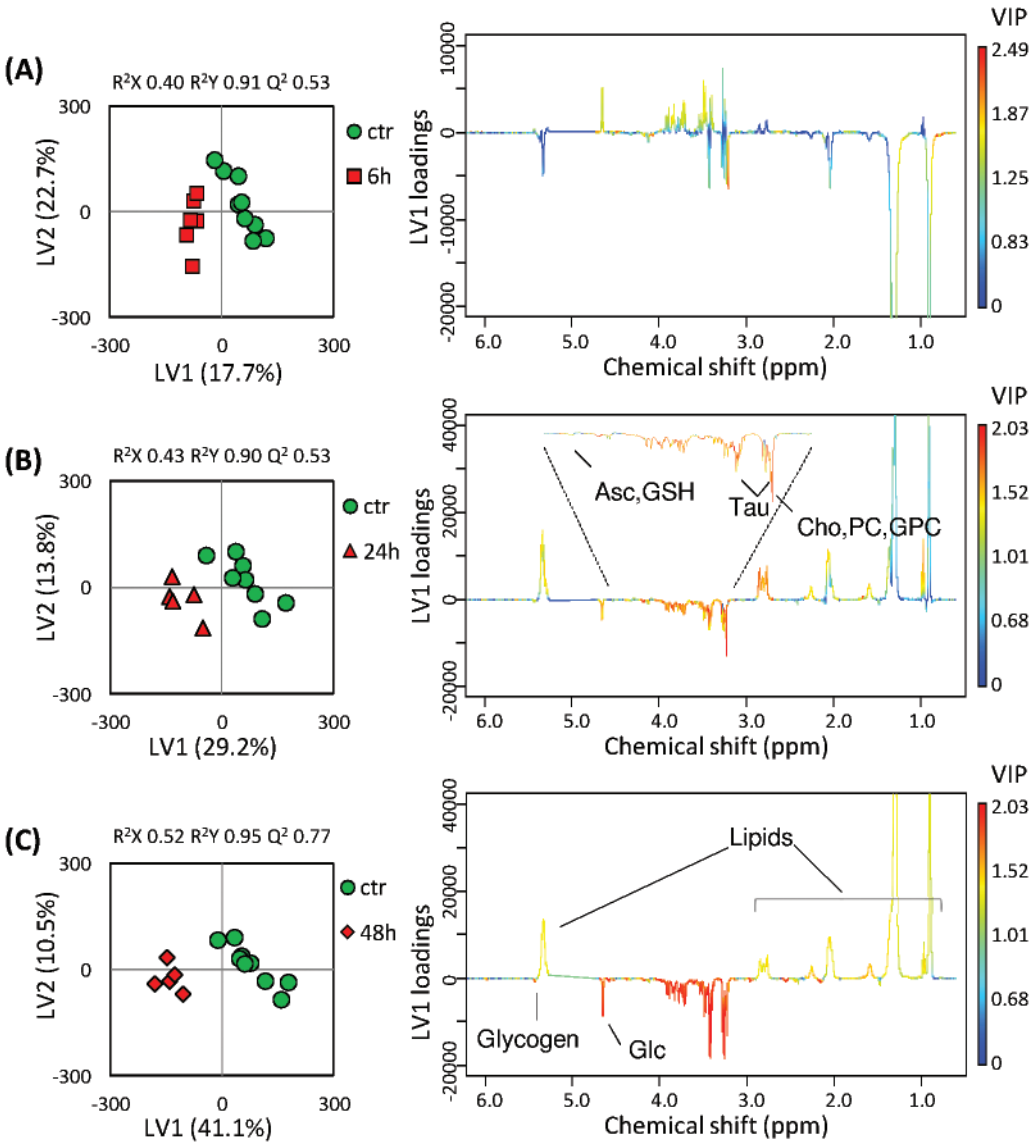

Figure 3. Scores scatter plots (left) and LV1 loadings (right) resulting from PLS-DA of ^{1}H T_2-edited NMR spectra of liver tissues from control and AgNPs-dosed mice at: (A) 6 h, (B) 24 h, and (C) 48 h postinjection. Loadings are colored according to VIP (vide online version) and some assignments are indicated. Abbreviations: Asc, ascorbate; Cho, choline; Glc, glucose; GPC, glycerophosphocholine; GSH, glutathione; PC, phosphocholine; Tau, taurine.

characterize the macromolecular profile. Typical serum spectra (standard, T_2-edited and diffusion-edited) are shown in Supplementary Figure 8 and signal assignment is reported in Supplementary Table 2.

The separation between the sera of control and dosed animals was apparent in the scores plots obtained by PCA and PLS-DA of all samples (Supplementary Figure 9), having been further explored by considering each postinjection period at a time, similarly to the approach used for tissues. The resulting PLS-DA scores and loadings (Figure 5) suggested important time-dependent changes in both macromolecules and small metabolites, the magnitude and significance of which were verified through spectral integration (Figure 4F). The macromolecular profiles of dosed mice showed decreased levels of very low-density lipoprotein (VLDL) and increased levels of HDL and glycoproteins, compared with controls. In terms of small metabolites, there were several time-dependent changes in glucose, organic acids (including significant decreases of lactate and pyruvate at 48 h postinjection), amino acids (including significant increases in lysine), creatine and phosphocreatine (significantly increased in the serum of 6 and 24 h dosed animals), among others (Figure 4F).

DISCUSSION

In this study, we have assessed the biological effects of AgNPs intravenously administered to mice through an integrated approach which combined conventional toxicity readouts (clinical chemistry and histopathology) with metabolic profiling (metabolomics) of major target organs and blood serum. The dose of AgNPs administered to mice (8 mg/kg bw) falls within the dose range previously tested on intravenously injected mice/rats without eliciting overt toxicity (De Jong *et al.*, 2013; Dziendzikowska *et al.*, 2012; Tiwari *et al.*, 2011; Xue *et al.*, 2012). Moreover, other *in vivo* studies have shown AgNPs to have biological activity, such as antiviral (Xiang *et al.*, 2013) and

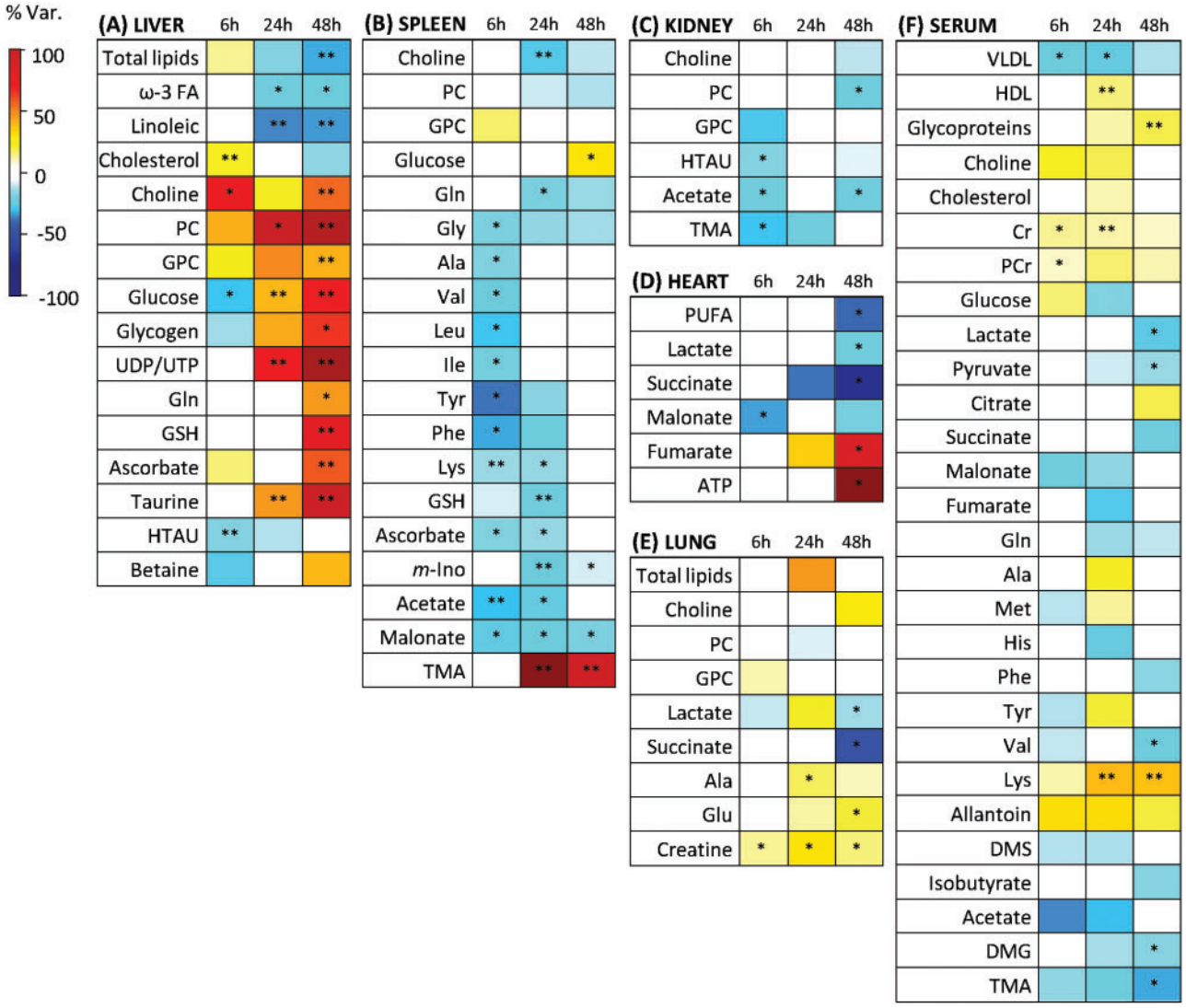

Figure 4. Heatmap showing the metabolic variations in the organs and serum of AgNPs-dosed mice, at 6, 24, and 48 h postinjection, in relation to controls: (A) liver; (B) spleen; (C) kidney; (D) heart; (E) lung; (F) blood serum. The scale is color-coded as a function of the % variation, from maximum decrease (dark blue) to maximum increase (dark red) (vide online version). The criterium for including a metabolite in the heatmap was absolute ES > 0.5 (and SE < ES). Statistically significant differences are indicated (*$p < .05$, **$p < .01$). Abbreviations: ATP, adenosine triphosphate; Cr, creatine; DMG, dimethylglycine; DMS, dimethylsulfone; FA, fatty acids; GPC, glycerophosphocholine; GSH, reduced glutathione; HDL, high-density lipoproteins; HTAU, hypotaurine; *m*-Ino, *myo*-inositol; PC, phosphocholine; PCr, phosphocreatine; PUFA, polyunsaturated fatty acids; TMA, trimethylamine; UDP/UTP, uridine di/triphosphate; VLDL, very low-density lipoproteins; 3 letter code used for amino acids.

anticancer activity (Swanner *et al.*, 2015), at similar or lower dosages (1–5 mg/kg bw), thus confirming the relevance of the dose used in this study. It is also important to note that, according to the guidelines for dosage conversion from animals to humans (Reagan-Shaw *et al.*, 2007), the equivalent human dose is 0.65 mg/kg bw, corresponding to 38.9 mg AgNPs in an adult subject of 60 kg. Serum silver levels in humans exposed to burn dressings containing AgNPs were reported to be in the 50–500 μg/l range (Moiemen *et al.*, 2011; Vlachou *et al.*, 2007), corresponding to 0.2–2.2 mg Ag in an adult subject with 60 kg (estimated blood volume of 4.5 l). Hence, the dose used in our study is also relevant in the context of human exposure to AgNPs-containing products.

Under the experimental conditions considered, the NP-dosed mice showed normal behavior and no evidence of gross toxicity. Hematological analysis showed a transient inversion of the leucocyte formula, possibly reflecting an inflammatory reaction, but all other parameters were similar to control animals. Serum biochemistry further showed trends for altered levels of triglycerides and HDL cholesterol, while the levels of enzymes commonly used as indicators of hepatobiliary toxicity (Ozer *et al.*, 2008) were similar in control and treated mice. At the histopathological level, with the exception of heart, which displayed normal microanatomic features, the other organs were moderately affected upon AgNPs exposure, exhibiting mild degenerative changes. One of such alterations was the cytoplasmic vacuolation of hepatocytes; interestingly, it has been reported that nonlipid, glycogen-filled cytoplasmic vacuolation, accompanied by an increase in total hepatic glycogen, could be a beneficial adaptation of hepatocytes towards a toxic insult (Nayak *et al.*, 1996). In this study, NMR analysis of liver tissue has indeed provided evidence for glycogen accumulation at 24 and 48 h postinjection. This information, together with the absence of elevated serum markers of hepatotoxicity, suggests

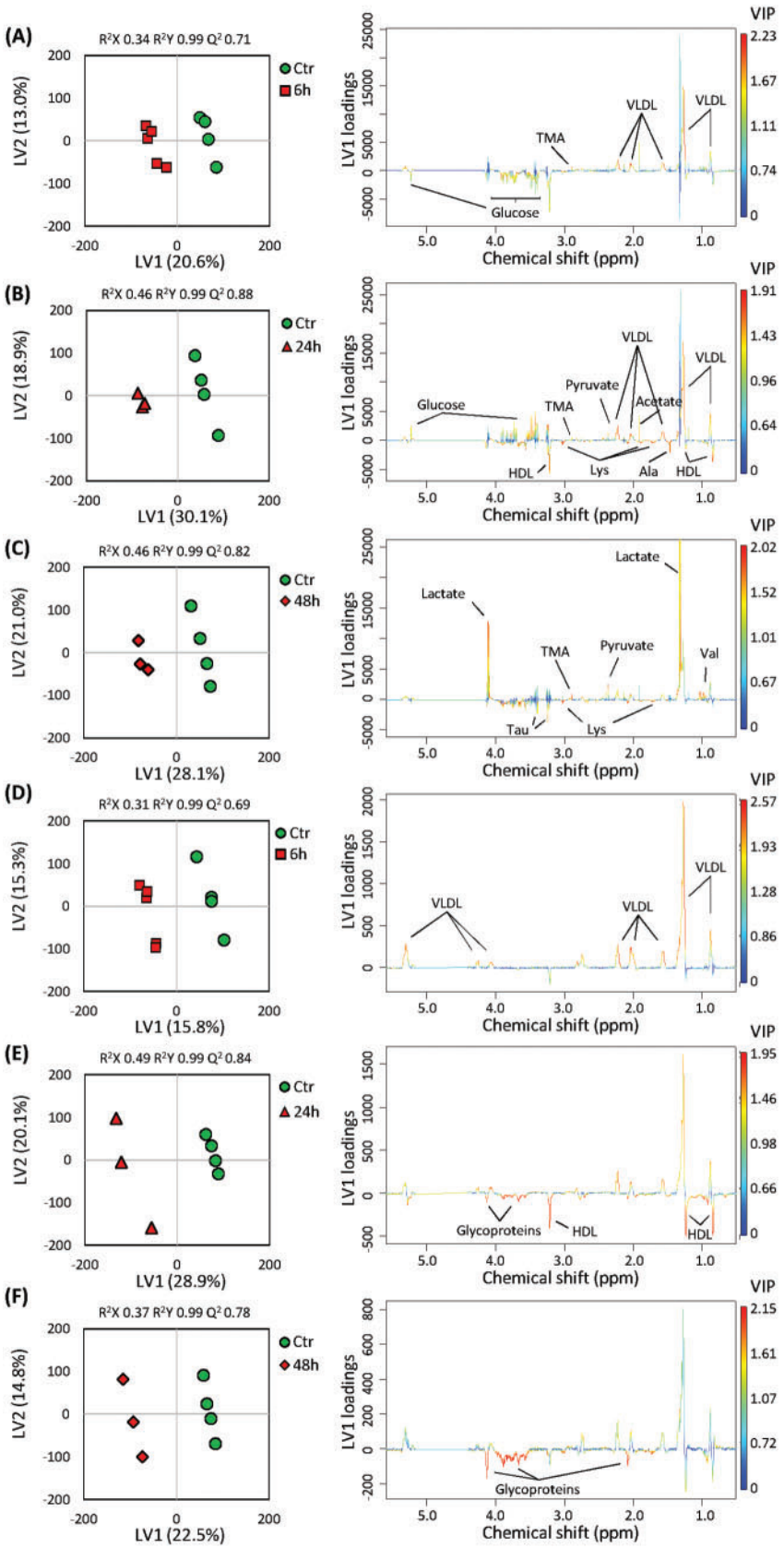

Figure 5. Scores scatter plots (left) and LV1 loadings (right) resulting from PLS-DA of ^{1}H T_2-edited (A–C) and of diffusion-edited (D–F) NMR spectra of blood serum from control and AgNPs-dosed mice at: (A,D) 6 h; (B), (E) 24 h; (C,F) 48 h postinjection. Loadings are colored according to VIP (vide online version) and some assignments are indicated. Abbreviations: HDL, high-density lipoproteins; TMA, trimethylamine; VLDL, very low-density lipoproteins; 3 letter code used for amino acids.

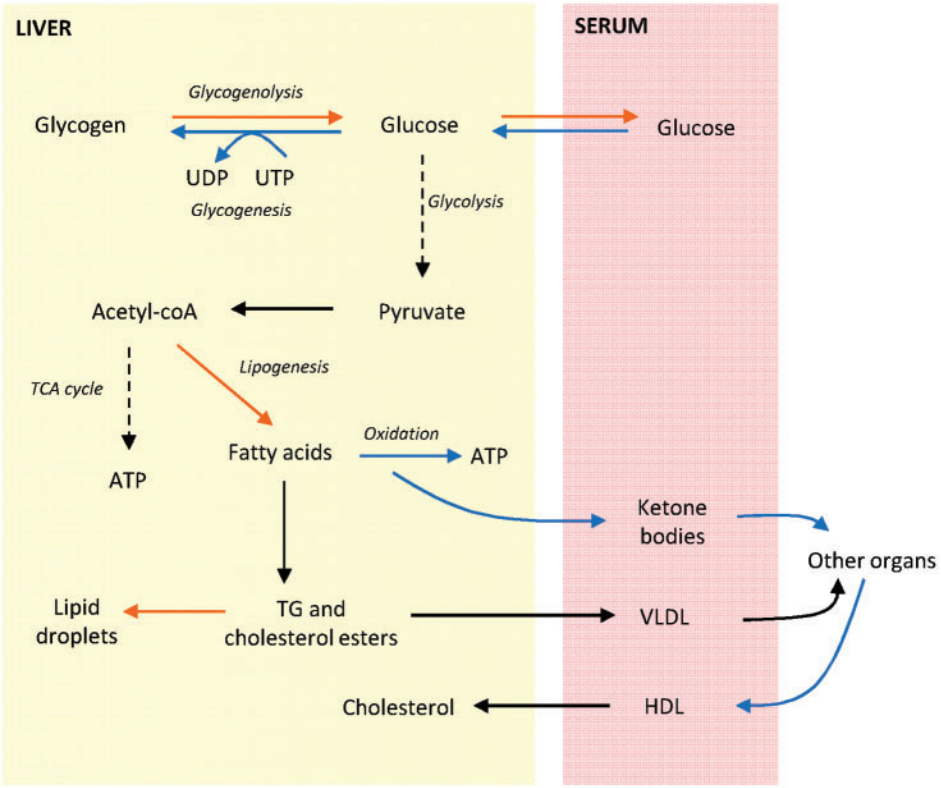

Figure 6. Schematic representation of glucose and lipid metabolism in liver and blood serum: the pathways suggested to be upregulated upon AgNPs exposure are indicated by the arrows in orange for 6 h postinjection and in blue for 24/48 h postinjection (vide online version).

that the hepatic histopathological changes observed were transient and did not reflect persistent liver injury. Overall, the lack of marked changes in blood parameters and histological features is in line with previous reports showing that AgNPs could be well tolerated when injected into mice or rats at doses < 10 mg/kg bw (Tiwari *et al.*, 2011; Xue *et al.*, 2012).

Metabolic profiling of animal tissues and serum allowed the changes in local and systemic metabolism to be monitored upon AgNPs exposure. Liver and spleen were the organs where AgNPs had the greatest metabolic impact, as indicated by the higher number and magnitude of variations relative to controls (Figure 4). This is consistent with these organs being the major sites of AgNPs accumulation following i.v. injection, as recurrently reported in the literature (Chrastina and Schnitzer, 2010; Recordati *et al.*, 2016; Wang *et al.*, 2013; Xue *et al.*, 2012), and based also on our silver biodistribution results (Supplementary Figure 2).

The hepatic variations related to lipids and carbohydrate metabolism indicated a 2-stage response (Figs. 4A and 6). At the earlier time postinjection (6 h), the observed decreases in glycogen and glucose, together with increases in total lipids and cholesterol, suggested upregulated glycogenolysis and lipid synthesis/storage in the liver of treated mice. Concomitantly, serum glucose was increased and VLDL lipoproteins were decreased, suggesting that lipids were preferentially stored in hepatocytes rather than being transported into the blood. Interestingly, glycogen depletion together with lipid accumulation, hereby observed as an early response to AgNPs, have been previously reported as major ultrastructural hepatocytic alterations related to AgNPs toxicity, possibly involving impairment of glycogen synthesis and of lipid catabolism and/or transport (Almansour *et al.*, 2016). Moreover, decreased hepatic glucose and glycogen levels have often been linked to the toxicity induced by other types of NPs, namely manganese NPs (Li *et al.*, 2014a; Jinquan *et al.*, 2013), ultrasmall iron oxide particles (Feng *et al.*, 2011), carbon nanotubes (Lin *et al.*, 2013) and silica NPs (Lu *et al.*, 2011, 2015). In this study, however, these effects appeared to be transient, since at longer postinjection times (24 and 48 h), the liver of treated mice showed elevated levels of glucose and glycogen (as well of UDP/UTP, needed for glycogen synthesis), and decreased amounts of total lipids (fatty acids, triglycerides and cholesterol). Along with decreased blood glucose levels, these findings suggest a metabolic shift towards glycogenesis, accompanied by lipolysis and fatty acid oxidation, which in turn may relate to decreased seric VLDL. On the other hand, serum HDL was found significantly increased at 24 h, as already indicated by serum biochemical assays, possibly reflecting increased reverse transport of cholesterol back into the liver.

The hepatic metabolic profile of treated mice additionally showed increased levels of choline compounds, right from the early postinjection time. Besides their role as membrane structural and signaling components, these molecules have been postulated as immune response regulators (Thompson *et al.*, 1999). Hence, as noted in a previous report of exposure to MnO NPs (Jinquan *et al.*, 2013), their increase may relate to the phagocytic removal of damaged liver cells. Also, antioxidative defense mechanisms appeared to be activated upon AgNPs exposure, as suggested by the increased levels of several antioxidant molecules (GSH, ascorbate and taurine) in the liver of treated mice, especially at 48 h postinjection. This agrees with the reported inverse correlation between liver GSH levels and the dose of AgNPs injected into rats (El Mahdy *et al.*, 2015), thus supporting the hypothesis of a protective response elicited by low levels of oxidative stress. Accordingly, we have observed up-regulated

GSH synthesis *in vitro*, to cope with the generation of reactive oxygen species, both in human keratinocytes (Carrola *et al.*, 2016a,b) and in liver cells (unpublished results). Finally, the variations in the levels of betaine, which may function as a methyl donor, are consistent with the importance of methylation reactions in proper liver function and detoxification reactions (Alirezaei *et al.*, 2014), as also noted by Li and co-authors in their study of MnO NPs (Jinquan *et al.*, 2013). The levels of other molecules with ability to carry and donate methyl groups (dimethylglycine, dimethylsulfone, trimethylamine) were also found altered in the serum. Taken together, our results suggest that liver metabolism played a crucial role in coping with the presence of AgNPs in the organism, possibly contributing to avoid major damages. This agrees with a recent study of low-dose subchronic (1 mg/kg bw over 1 month) exposure of rats to AgNPs, whereby alterations in hepatic mitochondria appeared to be accompanied by liver compensatory efforts to maintain energy production (Teodoro *et al.*, 2016).

The spleen is a peripheral lymphoid organ with several functions in red blood cell homeostasis, the immune system, and, as recently recognized, in metabolism and the endocrine system (Tarantino *et al.*, 2013). Upon AgNPs exposure, splenic metabolic composition varied in a clear time-dependent way, with the highest number of alterations being observed at 6 and 24 h, while only a few differences remained at 48 h postinjection (Figure 4B). One of the most striking features of the short-term response (6 h) was the depletion of several amino acids (including branched chain and aromatic amino acids). The spleen is normally rich in amino acids due to its role in hemoglobin recycling from senescent red blood cells; hence, the observed decrease in amino acid levels may reflect an impairment of this splenic function. Interestingly, an analogous result was reported in rats exposed to the fungal T2-toxin via oral gavage (Wan *et al.*, 2015). Other early effects in the spleen of AgNPs-treated mice were decreased levels of ascorbate and GSH, suggesting the onset of oxidative stress, similarly to what has been reported in the spleen of rats exposed to X-ray radiation (Jang *et al.*, 2016). Additionally, at 6 h postinjection, there was a non-significant increase in glycerophosphocholine, suggesting some degree of membrane disruption, and the levels of acetate and malonate were decreased in comparison to control mice. At 24 and/or 48 h postinjection, most amino acids recovered their normal levels, and so did ascorbate, GSH, glycerophosphocholine and acetate, indicating rescue from early perturbations in hemoglobin recycling, oxidative balance and lipid metabolism. At the same time, new changes emerged, namely decreased glutamine, myo-inositol, choline, and phosphocholine, together with increased trimethylamine and glucose. Given that splenic histological alterations were more prominent at later time points, these changes may be postulated to reflect adverse outcomes, although the clarification of this issue would require further investigation over an extended period of time. The strong increase in trimethylamine is especially intriguing as, to our knowledge, this metabolite, which can be formed from choline by gut bacterial enzymes (Zeisel *et al.*, 1989), has not been previously related to spleen metabolic composition and function.

AgNPs appeared to have moderate effects on the renal metabolic profile, with decreases being registered for choline compounds, hypotaurine, acetate and trimethylamine (Figure 4C). It is possible that these changes reflect disturbances in the osmoregulatory and excretory functions of the kidneys, similarly to the results reported for renal tissue of rats exposed to ultrasmall paramagnetic iron oxide particles (Feng *et al.*, 2011). However, changes in other putative nephrotoxicity markers (Boudonck *et al.*, 2009; Griffin *et al.*, 2000) were not detected, supporting the low impact of AgNPs on renal cell metabolism. One possible reason for this would be the low accumulation of AgNPs in the kidneys. Indeed, while the presence of AgNPs in the kidneys as early as 1 h postinjection (Supplementary Figure 2) suggests renal clearance to be an important excretion route for AgNPs, in accordance with other works (Dziendzikowska *et al.*, 2012; Wang *et al.*, 2013), it has been reported that, at longer postinjection times, the concentrations of AgNPs in the kidneys are much lower than those found in the liver, spleen, or lungs (Chrastina and Schnitzer, 2010; Recordati *et al.*, 2016; Chen *et al.*, 2016). Moreover, the high resilience of kidney mitochondria to damage, shown recently in AgNPs-exposed rats (Teodoro *et al.*, 2016), may also account for the lack of major renal metabolic changes.

The heart metabolic profile showed changes in metabolites involved in energy metabolism, especially at 48 h postinjection (Figure 4D). At 6 h postinjection the only relevant variation was a significant decrease in malonate. This metabolite is a competitive inhibitor of the enzyme succinate dehydrogenase (SDH) which catalyzes the conversion of succinate into fumarate in the TCA cycle (Potter and Dubois, 1943). Notably, malonate depletion at early exposure time seemed to have a determinant effect on heart metabolism at subsequent times, as indicated by decreased succinate and increased fumarate, possibly due to less inhibited SDH. This could have implied upregulation of the TCA cycle activity, as indeed corroborated by decreased lactate (pyruvate channeled into TCA rather than being converted to lactate), decreased fatty acids (used to produce acetyl-coA) and increased ATP production. Thus, based also on the observation that the heart of treated mice did not show histopathological alterations, we may hypothesize that the metabolic adaptation described earlier was an efficient protective mechanism, although the relation between AgNPs and the triggering of malonate depletion remains to be clarified.

The lungs of treated mice displayed changes in total lipids and choline compounds (Figure 4E), which, although not reaching statistical relevance, may relate to possible alterations in pulmonary surfactant composition and turnover, as observed before under the influence of cytokines released during inflammation (Akella and Deshpande, 2013). Additionally, the exposed lung tissue showed significant elevation of creatine, right from 6 h postinjection, as well as of alanine and glutamate (24/48 h), together with significantly reduced levels of lactate and succinate at 48 h postinjection. Creatine is a key intermediate in energy transfer processes, its increase often being associated with high energy demand. Also, high creatine levels have been postulated to have cytoprotective effects toward oxidative agents (Young *et al.*, 2010) and inflammation (Khanna and Madan, 1978). Thus, the creatine increase may eventually relate to the observed histopathological signs of AgNPs-induced inflammatory reactions in the lung. Interestingly, creatine and phosphocreatine were also found significantly increased in the blood serum of treated mice. The remaining pulmonary changes suggest downregulation of glycolysis (decreased lactate) and of the TCA cycle (decrease in succinate and increases in the TCA substrates alanine and glutamate), likely reflecting AgNPs-induced impairment of metabolic activity in inflamed lungs. However, to determine if these changes are transient or sustained in time, further studies at longer postinjection periods would be needed.

The composition of blood serum reflects the metabolic activity of the various organs, making it difficult to determine the specific origin of each seric metabolite or of its variation. Globally, upon AgNPs exposure, the serum metabolome showed

time-dependent changes in both macromolecular components (lipoproteins and glycoproteins, the latter being significantly increased at 48 h postinjection) and small metabolites, such as amino acids and derivatives, organic acids, methylated compounds and allantoin (Figure 4F). Allantoin is a diureide of glyoxylic acid resulting from the free radical-induced oxidation of uric acid, the terminal product of purine metabolism (Wishart *et al.*, 2007). Thus, its increased levels in serum may relate to oxidative stress, a well-established process in AgNPs-mediated toxicity (Dubey *et al.*, 2015; Kim and Ryu, 2013), also supported by some of our findings in tissues, as discussed earlier.

CONCLUSIONS

This study has provided insight into the metabolic adaptations undergone by various mice organs in response to AgNPs administered intravenously, at a dose not causing overt toxicity. Liver and spleen, the major target organs of AgNPs accumulation, showed a 2-stage response, where early metabolic changes suggestive of some functional impairments were followed by activation of protective mechanisms and organ recovery. This was particularly evident in the liver, where the upregulation of glycogenesis and lipolysis, together with increases in metabolites related to antioxidative defense, immunoregulation and detoxification, seemed to play a crucial role in avoiding major functional damage. The spleen also recovered from initial disturbances in amino acid, lipid and oxidative metabolism, although a number of other metabolite changes emerging at later time points, where histological alterations were more prominent, could eventually reflect some adverse effects. In the heart, the metabolic shift towards intensification of the TCA cycle and increased ATP production possibly reflected a beneficial adaptation that allowed this organ to cope with the presence of AgNPs. On the other hand, the TCA cycle appeared to be down regulated in the lungs of injected mice, which showed signs of inflammation. As for the kidneys, they showed the mildest metabolic response to AgNPs, with apparent moderate disturbances in osmoregulatory and excretory functions. Overall, this study has shown that intermediary metabolism not only responded sensitively to the presence of AgNPs, in an organ-specific and time-dependent way, as it played vital roles in protecting cells and mitigating toxic effects. The potential role of metabolism in governing toxicity opens new prospects for the development of strategies allowing for an improved control over cellular responses to NPs. Finally, it may be concluded that NMR metabolomics is a powerful tool to monitor multi-organ metabolic adaptations upon *in vivo* exposure to NPs, showing the ability to reveal unforeseen effects and to provide important mechanistic insights, not accessible through conventional toxicity assessments.

SUPPLEMENTARY DATA

Supplementary data are available at *Toxicological Sciences* online.

FUNDING

This work was developed within the scope of the project CICECO-Aveiro Institute of Materials, POCI-01-0145-FEDER-007679 (UID/CTM/50011/2013) and iMed.ULisboa (UID/DTP/04138/2013) financed by national funds through the FCT/MEC and when appropriate co-financed by FEDER under the PT2020 Partnership Agreement. Funding to the project FCOMP-01-0124-FEDER-021456 (PTDC/SAU-TOX/120953/2010) by FEDER through COMPETE and by national funds through FCT is acknowledged. J.C. and I.F.D. acknowledge FCT/MCTES for the grant (SFRH/BD/79494/2011) and the "IF2014" research contract, respectively.

ACKNOWLEDGMENTS

We acknowledge Prof. Ruth Duncan for insightful discussions and Dr Manfred Spraul, Bruker BioSpin (Germany) for access to software and spectral database. The Portuguese National NMR (PTNMR) Network, supported with FCT funds, is also acknowledged.

REFERENCES

Akella, A., and Deshpande, S. B. (2013). Pulmonary surfactants and their role in pathophysiology of lung disorders. *Indian J. Exp. Biol.* **51**, 5–22.

Alirezaei, M., Jelodar, G., Ghayemi, Z., and Mehr, M. K. (2014). Antioxidant and methyl donor effects of betaine versus ethanol-induced oxidative stress in the rat liver. *Comp. Clin. Path.* **23**, 161–168.

Almansour, M., Sajti, L., Melhim, W., and Jarrar, B. M. (2016). Ultrastructural hepatocytic alterations induced by silver nanoparticle toxicity. *Ultrastruct. Pathol.* **40**, 92–100.

Berben, L., Sereika, S. M., and Engberg, S. (2012). Effect size estimation: Methods and examples. *Int. J. Nurs. Stud.* **49**, 1039–1047.

Boudonck, K. J., Mitchell, M. W., Nemet, L., Keresztes, L., Nyska, A., Shinar, D., and Rosenstock, M. (2009). Discovery of metabolomics biomarkers for early detection of nephrotoxicity. *Toxicol. Pathol.* **37**, 280–292.

Carrola, J., Bastos, V., Ferreira De Oliveira, J. M. P., Oliveira, H., Santos, C., Gil, A. M., and Duarte, I. F. (2016a). Insights into the impact of silver nanoparticles on human keratinocytes metabolism through NMR metabolomics. *Arch. Biochem. Biophys.* **589**, 53–61.

Carrola, J., Bastos, V., Jarak, I., Oliveira-Silva, R., Malheiro, E., Daniel-da-Silva, A. L., Oliveira, H., Santos, C., Gil, A. M., and Duarte, I. F. (2016b). Metabolomics of silver nanoparticles toxicity in HaCaT cells: Structure–activity relationships and role of ionic silver and oxidative stress. *Nanotoxicology* **10**, 1105–1117.

Chen, R., Zhao, L., Bai, R., Liu, Y., Han, L., Xu, Z., Chen, F., Autrup, H., Long, D., and Chen, C. (2016). Silver nanoparticles induced oxidative and endoplasmic reticulum stresses in mouse tissues: Implications for the development of acute toxicity after intravenous administration. *Toxicol. Res.* **1**, 602–608.

Chrastina, A., and Schnitzer, J. E. (2010). Iodine-125 radiolabeling of silver nanoparticles for in vivo SPECT imaging. *Int. J. Nanomedicine* **5**, 653–659.

Cloarec, O., Dumas, M. E., Craig, A., Barton, R. H., Trygg, J., Hudson, J., Blancher, C., Gauguier, D., Lindon, J. C., Holmes, E., *et al.* (2005). Statistical total correlation spectroscopy: An exploratory approach for latent biomarker identification from metabolic 1H NMR data sets. *Anal. Chem.* **77**, 1282–1289.

Davenport, L. L., Hsieh, H., Eppert, B. L., Carreira, V. S., Krishan, M., Ingle, T., Howard, P. C., Williams, M. T., Vorhees, C. V., and Genter, M. B. (2015). Systemic and behavioral effects of intranasal administration of silver nanoparticles. *Neurotoxicol. Teratol.* **51**, 68–76.

De Jong, W. H., Van Der Ven, L. T. M., Sleijffers, A., Park, M. V. D. Z., Jansen, E. H. J. M., Van Loveren, H., and Vandebriel, R. J. (2013). Systemic and immunotoxicity of silver nanoparticles

in an intravenous 28 days repeated dose toxicity study in rats. *Biomaterials* **34**, 8333–8343.

Dieterle, F., Ross, A., Schlotterbeck, G., and Senn, H. (2006). Probabilistic quotient normalization as robust method to account for dilution of complex biological mixtures. Application in 1H NMR metabonomics. *Anal. Chem.* **78**, 4281–4290.

Duarte, I. F. (2011). Following dynamic biological processes through NMR-based metabonomics: A new tool in nanomedicine? *J. Control. Release* **153**, 34–39.

Dubey, P., Matai, I., Kumar, S. U., Sachdev, A., Bhushan, B., and Gopinath, P. (2015). Perturbation of cellular mechanistic system by silver nanoparticle toxicity: Cytotoxic, genotoxic and epigenetic potentials. *Adv. Colloid Interface Sci.* **221**, 4–21.

Dziendzikowska, K., Gromadzka-Ostrowska, J., Lankoff, A., Oczkowski, M., Krawczyńska, A., Chwastowska, J., Sadowska-Bratek, M., Chajduk, E., Wojewódzka, M., Dušinská, M., *et al.* (2012). Time-dependent biodistribution and excretion of silver nanoparticles in male Wistar rats. *J. Appl. Toxicol.* **32**, 920–928.

El Mahdy, M. M., Eldin, T. A. S., Aly, H. S., Mohammed, F. F., and Shaalan, M. I. (2015). Evaluation of hepatotoxic and genotoxic potential of silver nanoparticles in albino rats. *Exp. Toxicol. Pathol.* **67**, 21–29.

Feng, J., Liu, H., Bhakoo, K. K., Lu, L., and Chen, Z. (2011). A metabonomic analysis of organ specific response to USPIO administration. *Biomaterials* **32**, 6558–6569.

Ge, L., Li, Q., Wang, M., Ouyang, J., Li, X., and Xing, M. M. Q. (2014). Nanosilver particles in medical applications: Synthesis, performance, and toxicity. *Int. J. Nanomedicine* **9**, 2399–2407.

Griffin, J. L., Walker, L. A., Troke, J., Osborn, D., Shore, R. F., and Nicholson, J. K. (2000). The initial pathogenesis of cadmium induced renal toxicity. *FEBS Lett.* **478**, 147–150.

Hadrup, N., and Lam, H. R. (2014). Oral toxicity of silver ions, silver nanoparticles and colloidal silver - A review. *Regul. Toxicol. Pharmacol.* **68**, 1–7.

Hadrup, N., Lam, H. R., Loeschner, K., Mortensen, A., Larsen, E. H., and Frandsen, H. (2012). Nanoparticulate silver increases uric acid and allantoin excretion in rats, as identified by metabolomics. *J. Appl. Toxicol.* **32**, 929–933.

Jang, W. G., Park, J. Y., Lee, J., Bang, E., Kim, S. R., Lee, E. K., Yun, H. J., Kang, C.-M., and Hwang, G.-S. (2016). Investigation of relative metabolic changes in the organs and plasma of rats exposed to X-ray radiation using HR-MAS ^{1}H NMR and solution ^{1}H NMR. *NMR Biomed.* **29**, 507–518.

Jinquan, L., Zhenghuan, Z., Jianghua, F., Jinhao, G., and Zhong, C. (2013). Understanding the metabolic fate and assessing the biosafety of MnO nanoparticles by metabonomic analysis. *Nanotechnology* **24**, 455102.

Khanna, N. K., and Madan, B. (1978). Studies on the anti-inflammatory activity of creatine. *Arch. Int. Pharmacodyn. Ther.* **231**, 340–350.

Kim, S., and Ryu, D. Y. (2013). Silver nanoparticle-induced oxidative stress, genotoxicity and apoptosis in cultured cells and animal tissues. *J. Appl. Toxicol.* **33**, 78–89.

Korani, M., Rezayat, S. M., Gilani, K., Arbabi Bidgoli, S., and Adeli, S. (2011). Acute and subchronic dermal toxicity of nanosilver in guinea pig. *Int. J. Nanomedicine* **6**, 855–862.

Li, J., Zhou, Z., Feng, J., Cai, S., Gao, J., and Chen, Z. (2014a). NMR-based metabonomic analysis of MnO-embedded iron oxide nanoparticles as potential dual-modal contrast agents. *J. Nanoparticle Res.* **16**, 2411.

Li, L., Wu, H., Peijnenburg, W. J. G. M., and van Gestel, C. A. M. (2015a). Both released silver ions and particulate Ag contribute to the toxicity of AgNPs to earthworm Eisenia fetida. *Nanotoxicology* **9**, 792–801.

Li, L. Z., Wu, H., Ji, C., van Gestel, C. a M., Allen, H. E., and Peijnenburg, W. J. G. M. (2015b). A metabolomic study on the responses of daphnia magna exposed to silver nitrate and coated silver nanoparticles. *Ecotoxicol. Environ. Saf.* **119**, 66–73.

Li, Y., Bhalli, J. A., Ding, W., Yan, J., Pearce, M. G., Sadiq, R., Cunningham, C. K., Jones, M. Y., Monroe, W. a., Howard, P. C., *et al.* (2014b). Cytotoxicity and genotoxicity assessment of silver nanoparticles in mouse. *Nanotoxicology* **8(Suppl. 1)**, 36–45.

Lin, B., Zhang, H., Lin, Z., Fang, Y., Tian, L., Yang, H., Yan, J., Liu, H., Zhang, W., and Xi, Z. (2013). Studies of single-walled carbon nanotubes-induced hepatotoxicity by NMR-based metabonomics of rat blood plasma and liver extracts. *Nanoscale Res. Lett.* **8**, 236.

Lu, X., Ji, C., Jin, T., and Fan, X. (2015). The effects of size and surface modification of amorphous silica particles on biodistribution and liver metabolism in mice. *Nanotechnology* **26**, 175101.

Luo, C., Zhang, Y., Zeng, X., Zeng, Y., and Wang, Y. (2005). The role of poly(ethylene glycol) in the formation of silver nanoparticles. *J. Colloid Interface Sci.* **288**, 444–448.

Lu, X., Tian, Y., Zhao, Q., Jin, T., Xiao, S., and Fan, X. (2011). Integrated metabonomics analysis of the size-response relationship of silica nanoparticles-induced toxicity in mice. *Nanotechnology* **22**, 55101.

Lv, M., Huang, W., Chen, Z., Jiang, H., Chen, J., Tian, Y., Zhang, Z., and Xu, F. (2015). Metabolomics techniques for nanotoxicity investigations. *Bioanalysis* **7**, 1527–1544.

Martins, M. B. A. F., Corvo, M. L., Marcelino, P., Marinho, H. S., Feio, G., and Carvalho, A. (2014). New long circulating magnetoliposomes as contrast agents for detection of ischemia–reperfusion injuries by MRI. *Nanomedicine* **10**, 207–214.

Moiemen, N. S., Shale, E., Drysdale, K. J., Smith, G., Wilson, Y. T., and Papini, R. (2011). Acticoat dressings and major burns: Systemic silver absorption. *Burns* **37**, 27–35.

Nayak, N. C., Sathar, S. A., Mughal, S., Duttagupta, S., Mathur, M., and Chopra, P. (1996). The nature and significance of liver cell vacuolation following hepatocellular injury–An analysis based on observations on rats rendered tolerant to hepatotoxic damage. *Virchows Arch.* **428**, 353–365.

Ozer, J., Ratner, M., Shaw, M., Bailey, W., and Schomaker, S. (2008). The current state of serum biomarkers of hepatotoxicity. *Toxicology* **245**, 194–205.

Potter, V., and Dubois, K. (1943). Studies on the mechanism of hydrogen transport in animal tissues. *J. Gen. Physiol.* **26**, 391–404.

Reagan-Shaw, S., Nihal, M., and Ahmad, N. (2007). Dose translation from animal to human studies revisited. *faseb J.* **22**, 659–661.

Recordati, C., De Maglie, M., Bianchessi, S., Argentiere, S., Cella, C., Mattiello, S., Cubadda, F., Aureli, F., D'Amato, M., Raggi, A., *et al.* (2016). Tissue distribution and acute toxicity of silver after single intravenous administration in mice: Nano-specific and size-dependent effects. *Part. Fibre Toxicol.* **13**, 12.

Swanner, J., Mims, J., Carroll, D. L., Akman, S. a., Furdui, C. M., Torti, S. V., and Singh, R. N. (2015). Differential cytotoxic and radiosensitizing effects of silver nanoparticles on triple-negative breast cancer and non-triple-negative breast cells. *Int. J. Nanomedicine* **10**, 3937–3953.

Tarantino, G., Scalera, A., and Finelli, C. (2013). Liver-spleen axis: Intersection between immunity, infections and metabolism. *World J. Gastroenterol.* **19**, 3534–3542.

Teodoro, J. S., Silva, R., Varela, A. T., Duarte, F. V., Rolo, A. P., Hussain, S., and Palmeira, C. M. (2016). Low-dose, subchronic exposure to silver nanoparticles causes mitochondrial alterations in Sprague–Dawley rats. *Nanomedicine* **11**, 1359–1375.

Thompson, D., Pepys, M. B., and Wood, S. P. (1999). The physiological structure of human C-reactive protein and its complex with phosphocholine. *Structure* **7**, 169–177.

Tiwari, D. K., Jin, T., and Behari, J. (2011). Dose-dependent in-vivo toxicity assessment of silver nanoparticle in Wistar rats. *Toxicol. Mech. Methods* **21**, 13–24.

Tran, Q. H., Nguyen, V. Q., and Le, A.-T. (2013). Silver nanoparticles: Synthesis, properties, toxicology, applications and perspectives. *Adv. Nat. Sci. Nanosci. Nanotechnol.* **4**, 33001.

Veselkov, K. A., Lindon, J. C., Ebbels, T. M. D., Crockford, D., Volynkin, V. V., Holmes, E., Davies, D. B., and Nicholson, J. K. (2009). Recursive segment-wise peak alignment of biological 1H NMR spectra for improved metabolic biomarker recovery. *Anal. Chem.* **81**, 56–66.

Vlachou, E., Chipp, E., Shale, E., Wilson, Y. T., Papini, R., and Moiemen, N. S. (2007). The safety of nanocrystalline silver dressings on burns: A study of systemic silver absorption. *Burns* **33**, 979–985.

Wan, Q., Wu, G., He, Q., Tang, H., and Wang, Y. (2015). The toxicity of acute exposure to T-2 toxin evaluated by the metabonomics technique. *Mol. BioSyst. Mol. BioSyst.* **11**, 882–891.

Wang, B., He, X., Zhang, Z., Zhao, Y., and Feng, W. (2013). Metabolism of nanomaterials in vivo: Blood circulation and organ clearance. *Acc. Chem. Res.* **46**, 761–769.

Wei, L., Lu, J., Xu, H., Patel, A., Chen, Z. S., and Chen, G. (2015). Silver nanoparticles: Synthesis, properties, and therapeutic applications. *Drug Discov. Today* **20**, 595–601.

Wishart, D. S., Tzur, D., Knox, C., Eisner, R., Guo, A. C., Young, N., Cheng, D., Jewell, K., Arndt, D., Sawhney, S., *et al.* (2007). HMDB: The Human Metabolome Database. *Nucleic Acids Res.* **35**, D521–D526.

Xiang, D., Zheng, Y., Duan, W., Li, X., Yin, J., Shigdar, S., O'Connor, M. L., Marappan, M., Zhao, X., Miao, Y., *et al.* (2013). Inhibition of A/Human/Hubei/3/2005 (H3N2) influenza virus infection by silver nanoparticles in vitro and in vivo. *Int. J. Nanomedicine* **8**, 4103–4114.

Xu, T., Zhang, N., Nichols, H. L., Shi, D., and Wen, X. (2007). Modification of nanostructured materials for biomedical applications. *Mater. Sci. Eng. C* **27**, 579–594.

Xue, Y., Zhang, S., Huang, Y., Zhang, T., Liu, X., Hu, Y., Zhang, Z., and Tang, M. (2012). Acute toxic effects and gender-related biokinetics of silver nanoparticles following an intravenous injection in mice. *J. Appl. Toxicol.* **32**, 890–899.

Young, J. F., Larsen, L. B., Malmendal, A., Nielsen, N., Straadt, I. K., Oksbjerg, N., and Bertram, H. C. (2010). Creatine-induced activation of antioxidative defence in myotube cultures revealed by explorative NMR-based metabonomics and proteomics. *J. Int. Soc. Sports Nutr.* **7**, 9.

Zeisel, S. H., DaCosta, K. a., Youssef, M., and Hensey, S. (1989). Conversion of dietary choline to trimethylamine and dimethylamine in rats: Dose-response relationship. *J. Nutr.* **119**, 800–804.